Electronic excitation of carbon monoxide by low-energy electron impact

Qiyan Sun,* Carl Winstead, and Vincent McKoy
A. A. Noyes Laboratory of Chemical Physics, California Institute of Technology, Pasadena, California 91125
(Received 20 July 1992)

Studies of the cross sections for electron-impact excitation of the valence states of carbon monoxide, i.e., the $a\,^3\Pi$, $A\,^1\Pi$, $a'\,^3\Sigma^+$, $e\,^3\Sigma^-$, $d\,^3\Delta$, $I\,^1\Sigma^-$, and $D\,^1\Delta$ states, have been carried out using the Schwinger multichannel variational method. Both differential and integral cross sections are obtained and compared with available experimental data. Reasonable agreement between the present results and experiment is seen for most of the states, and some differences are discussed. Estimates of the total cross section for electronic excitation of CO by low-energy electrons are provided.

PACS number(s): 34.80.Gs

I. INTRODUCTION

Electronic excitation and subsequent dissociation of carbon monoxide by low-energy impact play an important role in the modeling of lasers, gas discharges, plasmas, and reentry physics [1–3]. However, the data base of these excitation cross sections is still very fragmentary [4,5]. For the valence electronic states of interest in this work, only limited excitation functions for some states, measured in either emission or metastable detection experiments, are available [6–16]. Trajmar has reported preliminary results for the angular distributions for excitation of some valence electronic states at collision energies of 12.5 and 15 eV [17]. On the other hand, theoretical studies have so far been limited to low-order theories. Chung and Lin reported cross sections for excitation of several states of CO using the Born-Ochkur-Rudge (BOR) approximation [18], as did Lee and McKoy using the distorted-wave (DW) approximation [19]. These theories are not in good agreement with each other nor with experiment at low energies and are known to be subject to large uncertainties in this energy range.

We have formulated and exploited the Schwinger multichannel (SMC) variational method to determine the cross sections for electron-molecule collisions [20–22]. Implementation on highly parallel computers of the computational procedure for SMC calculations of these cross sections [23] has greatly facilitated studies of both elastic and electronically inelastic electron-molecule collisions. Recently, we have reported electron-impact excitation cross sections for the $a\,^3B_{1u}$ ($\pi\rightarrow\pi^*$) state of ethylene [24] and for the $a\,^3A_2$ and $A\,^1A_2$ states of formaldehyde [25], and elastic static-exchange cross sections for a number of polyatomic molecules [26]. In this paper, we present both integral and differential electron-impact excitation cross sections of the valence states of CO, i.e., the $a\,^3\Pi$, $A\,^1\Pi$, $a'\,^3\Sigma^+$, $e\,^3\Sigma^-$, $d\,^3\Delta$, $I\,^1\Sigma^-$, and $D\,^1\Delta$ states. These cross sections are compared with available experimental data and the results of other calculations.

In the next section the theoretical methods used are briefly summarized, while in Sec. III the numerical procedures are described. The results and discussion of these results are presented in Sec. IV, and a summary and conclusions are given in Sec. V.

II. THEORETICAL METHOD

The details of the SMC formulation have been given before [20] and are not repeated here. Here we give only a few key equations to facilitate subsequent discussions. The full SMC scattering amplitude in the linear momentum representation is given by

$$f^{\mathrm{SMC}}(\mathbf{k}_{\Gamma'},\mathbf{k}_{\Gamma})=-\frac{1}{2\pi}\sum_{m,n}\langle S_{\mathbf{k}_{\Gamma'}}|V|\Phi_m\rangle(d^{-1})_{mn}\times\langle\Phi_n|V|S_{\mathbf{k}_{\Gamma}}\rangle\ , \tag{1a}$$

where

$$d_{mn}=\left\langle\Phi_m\left|\frac{\hat{H}}{N+1}-\frac{P\hat{H}+\hat{H}P}{2}+\frac{PV+VP}{2}-VG_P^+V\right|\Phi_n\right\rangle\ . \tag{1b}$$

In Eq. (1), $S_{\mathbf{k}}$ is a product of a target eigenfunction and a plane wave $e^{i\mathbf{k}\cdot\mathbf{r}}$, V is the interaction potential, Φ_m is an $(N+1)$-electron determinant built on L^2 trial functions, $\hat{H}$ is the total energy minus the Hamiltonian of the system, N is the total number of electrons in the target, P is a projection operator on the open electronic channels of the target, and G_P^+ is the projected Green's function [20].

The integral cross section in the linear momentum representation is given by

$$\sigma_F^{\mathrm{SMC}}(k_{\Gamma'},k_{\Gamma})=\frac{k_{\Gamma'}}{k_{\Gamma}}\int\int|f^{\mathrm{SMC}}(\mathbf{k}_{\Gamma'},\mathbf{k}_{\Gamma})|^2d\hat{\mathbf{k}}_{\Gamma'}d\hat{\mathbf{k}}_{\Gamma}\ , \tag{2}$$

where $\hat{\mathbf{k}}_{\Gamma'(\Gamma)}$ are directions of the outgoing (incoming) plane waves. Transformation of the scattering amplitude

from the linear momentum representation to the angular momentum representation leads to the partial wave amplitude in the body-fixed frame,

$$f^{\mathrm{SMC}}_{l'm',lm}(k_{\Gamma'},k_\Gamma)=\int\int Y^*_{l'm'}(\hat{\mathbf{k}}_{\Gamma'})f^{\mathrm{SMC}}(k_{\Gamma'},k_\Gamma)\times Y_{lm}(\hat{\mathbf{k}}_\Gamma)d\hat{\mathbf{k}}_{\Gamma'}d\hat{\mathbf{k}}_\Gamma\ , \tag{3}$$

where Y_{lm} is a spherical harmonic. The integral cross section in the angular momentum representation is given by

$$\sigma_P^{\mathrm{SMC}}(k_{\Gamma'},k_\Gamma)=\frac{k_{\Gamma'}}{k_\Gamma}\sum_{l=0}^{l_{\max}}\sum_{m=-l}^{l}\sum_{l'=0}^{l_{\max}}\sum_{m'=-l'}^{l'}|f^{\mathrm{SMC}}_{l'm',lm}(k_{\Gamma'},k_\Gamma)|^2\ . \tag{4}$$

σ_F^{SMC} contains all the partial wave contributions, while σ_P^{SMC} is the integral cross section truncated at partial wave $l=l_{\max}$. The SMC differential cross section can be obtained from either Eq. (1) or Eq. (3). The procedure is straightforward and we will not give details here.

For electric-dipole-forbidden transitions, the interaction potential is of short range and hence an L^2 expansion of the trial scattering function in the SMC procedure would be adequate to describe the low partial waves which are the dominant contributions to the cross sections at the energies of interest here. However, such an L^2 expansion is not adequate for the higher partial waves that must be included for dipole-allowed transitions. For such dipole-allowed transitions an obvious strategy is to obtain the lower partial wave scattering amplitudes using the SMC approach and to approximate the higher-partial wave amplitudes by the first Born approximation (FBA) [27]. The full scattering amplitudes are then obtained by combining the SMC and the FBA amplitudes.

For scattering by a dipole potential, the scattering amplitude can be evaluated analytically in the FBA. In the linear momentum representation the FBA amplitude is given by [28]

$$f^{\mathrm{FBA}}(\mathbf{k}_{\Gamma'},\mathbf{k}_\Gamma)=2i\frac{\mathbf{D}\cdot(\mathbf{k}_{\Gamma'}-\mathbf{k}_\Gamma)}{|\mathbf{k}_{\Gamma'}-\mathbf{k}_\Gamma|^2}\ , \tag{5}$$

where $\mathbf{D}$ is the transition dipole moment and $\mathbf{k}_{\Gamma(\Gamma')}$ is the incoming (outgoing) wave vector. In the angular momentum representation the FBA amplitude becomes

$$f^{\mathrm{FBA}}_{l'm',lm}(k_{\Gamma'},k_\Gamma)=16|\mathbf{D}|(-1)^{m'}[(2l+1)(2l'+1)]^{1/2}\times(\pi^3/3)^{1/2}\begin{bmatrix}l & l' & 1\\ 0 & 0 & 0\end{bmatrix}\begin{bmatrix}l & l' & 1\\ m & -m' & m'-m\end{bmatrix}\times Y^*_{l,m'-m}(\hat{\mathbf{D}})I_{l'l}(k_{\Gamma'},k_\Gamma)\ , \tag{6}$$

where

$$I_{l'l}(k_{\Gamma'},k_\Gamma)=\frac{2^p}{(k_{\Gamma'}k_\Gamma)^{1/2}}\kappa^{p+(3/2)}\times\sum_{j=0}^{\infty}\frac{(2j+1)!!}{j!}\frac{(p+j)!}{[2(p+j)+3]!!}\kappa^{2j}\ , \tag{7}$$

with $p=l$ if $k_\Gamma>k_{\Gamma'}$, $p=l'$ if $k_{\Gamma'}>k_\Gamma$, and $\kappa=k_<\!/k_>$, where $k_<$ ($k_>$) is the smaller (larger) of k_Γ and $k_{\Gamma'}$.

Combination of the SMC and FBA amplitudes gives the scattering amplitude for dipole-allowed transitions,

$$f^{\mathrm{COM}}(\mathbf{k}_{\Gamma'},\mathbf{k}_\Gamma)=f^{\mathrm{FBA}}(\mathbf{k}_{\Gamma'},\mathbf{k}_\Gamma)+\sum_{l=0}^{l_{\max}}\sum_{m=-l}^{l}\sum_{l'=0}^{l_{\max}}\sum_{m'=-l'}^{l'}[f^{\mathrm{SMC}}_{l'm',lm}(k_{\Gamma'},k_\Gamma)-f^{\mathrm{FBA}}_{l'm',lm}(k_{\Gamma'},k_\Gamma)]Y_{l'm'}(\hat{\mathbf{k}}_{\Gamma'})Y^*_{lm}(\hat{\mathbf{k}}_\Gamma)\ . \tag{8}$$

The combined differential cross section may be obtained by

$$\frac{d\sigma^{\mathrm{COM}}(k_{\Gamma'},k_\Gamma)}{d\Omega}=\frac{k_{\Gamma'}}{k_\Gamma}\int\frac{d\alpha\sin\beta d\beta d\gamma}{8\pi^2}|f^{\mathrm{COM}}(\mathbf{k}_{\Gamma'},\mathbf{k}_\Gamma)|^2\ , \tag{9}$$

where α, β, and γ are Euler angles. The corresponding integral cross section is given by

$$\sigma^{\mathrm{COM}}(k_{\Gamma'},k_\Gamma)=\int\frac{d\sigma^{\mathrm{COM}}(k_{\Gamma'},k_\Gamma)}{d\Omega}d\Omega\ . \tag{10}$$

The above procedure for calculating cross sections for dipole-allowed transitions has also been used recently by Rescigno and Schneider [29]. The convergence of this procedure is quite fast, as will be seen below.

III. CALCULATIONS

In this study all target states are approximated by single-configuration wave functions. The ground-state wave function was obtained at the SCF level using Dunning's $(9s5p)/[5s3p]$ set [30] augmented by additional s, p, and d Gaussian functions for a total of 84 contracted Gaussians. The exponents of the additional Gaussian functions are given in Table I. This large basis set is not necessary for describing the target states at the SCF level but is needed for constructing the scattering wave function. The ground-state SCF energy in this basis at the internuclear distance of 2.132 a.u. was -112.778 a.u., compared to the Hartree-Fock limit of -112.786 a.u. [31]. The ground-state dipole moment was -0.122 a.u., which is in good agreement with the Hartree-Fock limit of -0.108 a.u. [31]; the corresponding experimental value is 0.044 a.u. [32]. The wave functions for the excited states were obtained using the improved virtual orbital (IVO) approach [33] in the same basis set and at the same internuclear distance. The vertical excitation energies are compared to the experimental values [34–36] in Table II, and good agreement is seen. For the dipole-allowed $X\,^1\Sigma^+\rightarrow A\,^1\Pi$ transition, our calculated dipole transition moment at the internuclear distance of 2.132 a.u. is 0.653 a.u., compared to the value 0.754 a.u. of Chantranupong *et al.*, obtained from a large

TABLE I. Exponents of additional Cartesian Gaussian functions.

Center	Type	Exponents
Carbon	s	0.61 32
	p	0.045 84
	d	1.5,0.75,0.3
Oxygen	s	0.113 84
	p	0.085 48
	d	1.7,0.85,0.34
Center of Mass	d	0.9,0.3

configuration-interaction calculation [37]. The corresponding value derived from experiment is 0.669 a.u. [38].

The cross sections for the $X\,^1\Sigma^+ \rightarrow a\,^3\Pi$ and $X\,^1\Sigma^+ \rightarrow A\,^1\Pi$ excitations are obtained from a five-channel calculation (counting the degenerate Π components separately). Below the singlet state threshold, the singlet state was included as a closed channel in this calculation. The excitation cross section for the $a\,^3\Pi$ state from a three-channel calculation differs only slightly from the corresponding result of a five-channel calculation. This agreement between the cross sections from three- and five-channel calculations stems partly from the large energy gap (about 3.5 eV) between the excitation thresholds. The results from the five-channel calculation will be presented in the next section.

The $X\,^1\Sigma^+ \rightarrow A\,^1\Pi$ excitation is the only dipole-allowed transition considered here, and the FBA must be used to include the higher partial wave contributions to the cross section. We included partial waves with $m \leq 2$ (due to the limitations of the basis set) and $l \leq 4$, 5, or 6 from the SMC calculation, with contributions from higher l and m taken from the FBA. The cross sections obtained with the different l cutoffs for the SMC contribution agreed within 1% or better with each other. We included partial waves up to $m=2$ and $l=5$ from the SMC calculation in the results reported below.

For the other cross sections, the $X\,^1\Sigma^+$, $a'\,^3\Sigma^+$, $e\,^3\Sigma^-$, $d\,^3\Delta$, $I\,^1\Sigma^-$, and $D\,^1\Delta$ states were coupled, resulting in a nine-channel calculation. These excited states all arise from the $(\pi \rightarrow \pi^*)$ excitation and can be expected to be strongly coupled. The excitation energies of the $d\,^3\Delta$ and $D\,^1\Delta$ states, i.e., 8.84 and 10.14 eV, were used as the common thresholds for the triplet and singlet states, respectively. The threshold energy of the $d\,^3\Delta$ state is about the average of those of the $a'\,^3\Sigma^+$ and $e\,^3\Sigma^-$ states, while the threshold energy of the $D\,^1\Delta$ state is only 0.43 eV above that of the $I\,^1\Sigma^-$ state. We tested other common threshold energies and observed minor effects on the physical cross sections.

The variational trial wave functions for the SMC are taken as linear combinations of spin-adapted $(N+1)$-electron Slater determinants. These determinants were constructed by antisymmetrizing the product of a target wave function and a scattering orbital, the latter being an IVO orbital. All the IVO's were used in building Slater determinants. To obtain converged results, a number of basis sets were tried. We kept the Dunning basis set fixed, and tested the convergence of the scattering basis by adding several additional Gaussian functions at a time and repeating the entire scattering calculation. This procedure was continued until the cross sections from successive basis sets were with a few percent of one another. The final set of additional Gaussian functions used is given in Table I.

In these calculations it was important to monitor the condition number of the matrix d_{mn} when solving the system of linear equations associated with Eq. (1). Numerical techniques previously described [25,39], based on singular-value decomposition, were used to eliminate instabilities associated with poor conditioning.

IV. RESULTS AND DISCUSSION

A. $a\,^3\Pi$ state

The excitation cross section for this state is shown in Fig. 1. For comparison, the results of three experimental measurements are also plotted in the same figure. Brongersma, Boerboom, and Kistemaker reported absolute values for their measured integral cross section [6]. The relative excitation function of Newman, Zubek, and King, which was measured in a metastable-detection experiment [7], is normalized to the maximum value of our calculated cross sections. The cross sections of Ajello were derived from emission experiments [8]. All four cross sections show a rapid rise in the threshold region, in qualitative agreement with one another. The calculated excitation function shows a maximum around 10.5 eV, about 4.5 eV above threshold. The data of Newman, Zubek, and King show a maximum in the cross sections at 9 eV, while that of Ajello peaks at 10.5 eV. Beyond this maximum, all three excitation functions decrease slowly and are in qualitative agreement with one another; all show characteristics of singlet-to-triplet excitation. At higher electron energies, the values of Newman, Zubek, and King seem too high, partly due to the contribution of

TABLE II. Vertical excitation energies for CO (eV).

State	Present results	Experiment	Reference
$a\,^3\Pi$	6.00	6.3	35
$a'\,^3\Sigma^+$	7.94	8.4	35
$e\,^3\Sigma^-$	9.71	9.7	35
$d\,^3\Delta$	8.84	9.2	35
$A\,^1\Pi$	9.52	8.35	34
$I\,^1\Sigma^-$	9.71	9.9	35
$D\,^1\Delta$	10.14	10.4	36

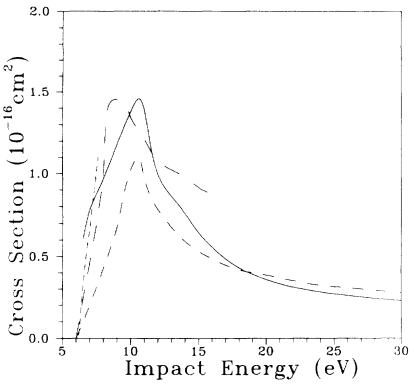

FIG. 1. Integral cross sections (excitation functions) for the $X\,^1\Sigma \rightarrow a\,^3\Pi$ electronic excitation of CO. The solid line is the present result, the short-dashed line is the result of Ref. [6], the medium-dashed line is the result of Ref. [8], and the long-dashed line is the result of Ref. [7].

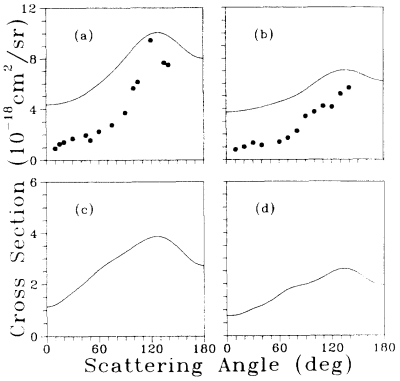

FIG. 3. Differential cross sections for the $X\,^1\Sigma \rightarrow a\,^3\Pi$ excitation of CO at impact energies (a) 12.5 eV; (b) 15 eV; (c) 20 eV; (d) 30 eV. The solid lines are the present results, and the dots are the measurements of Ref. [17].

higher-lying metastable states, as will be discussed further. Our excitation function agrees well with that of Ajello in shape and, at higher energies, in magnitude, but the two curves are significantly different in the near-threshold region. However, the error in the measurement of Ajello is estimated to be as large as 75% in magnitude, so this disagreement may not be significant.

The $a\,^3\Pi$ state has also been studied by Chung and Lin [18] in the BOR approximation and by Lee and McKoy [19] in the DW approximation. The BOR cross sections of Chung and Lin are too small compared to the measurements of Ajello between 10 and 30 eV, i.e., 50% smaller at 10 and 30 eV and 30% smaller at 20 eV. The DW cross sections of Lee and McKoy are in good agreement with Ajello's measurement at 30 eV but are as much as 40% larger at 20 eV.

The differential cross sections at selected energies are shown in Figs. 2 and 3. The experimental measurements of Trajmar at 12.5 and 15 eV [17] are also shown in Fig. 3. The agreement between theory and experiment is encouraging. Near threshold the calculated differential cross sections are fairly isotropic, reflecting the character of low partial waves. With increasing electron energy, backward scattering becomes more pronounced, as seen frequently for singlet-to-triplet excitation.

B. $A\,^1\Pi$ state

The integral excitation cross section for this state is shown in Fig. 4, along with the experimental data of Ajello [8] and of Mumma, Stone, and Zipf [9]. The excitation functions of Ajello were measured in an emission experiment and given on an absolute scale. Mumma, Stone, and Zipf measured electron-impact excitation cross sections for the lowest five vibrational levels of the $A\,^1\Pi$ state. For comparison, we plot the sum of these vibrational excitation cross sections in Fig. 4. All three curves show a broad maximum around 25 eV, in rough agreement with one another. The two sets of experimental measurements are in good agreement with each other above 18 eV. Our calculated excitation function lies between these two sets of experimental measurements in the near-threshold region, but is much too large at higher energies. However, comparison of our calculated differential and total cross sections with experimental

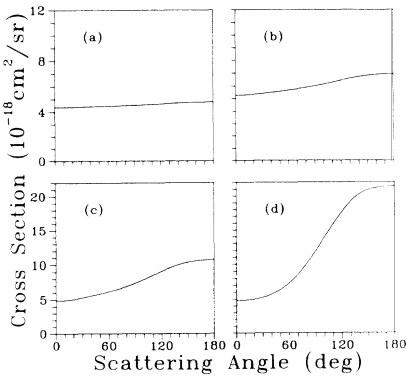

FIG. 2. Present differential cross sections for the $X\,^1\Sigma \rightarrow a\,^3\Pi$ excitation of CO at impact energies (a) 6.5 eV; (b) 7 eV; (c) 8 eV; (d) 10 eV.

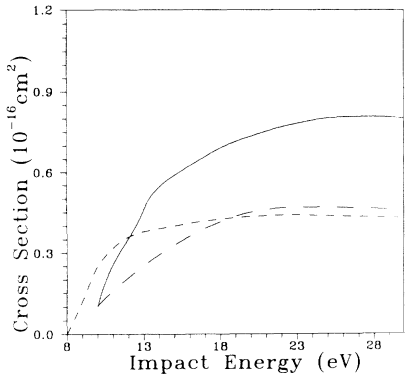

FIG. 4. Integral cross sections for the $X\,^1\Sigma \rightarrow A\,^1\Pi$ excitation of CO. The solid line is the present result, the short-dashed line is the result of Ref. [8], and the long-dashed line is the result of Ref. [9].

measurements suggests that the magnitude of our excitation function is reasonable.

Previous calculations of the cross sections for this state were done by Chung and Lin [18] and by Lee and McKoy [19]. A peak value of 1.4×10^{-16} cm^2 at 20 eV was obtained by Chung and Lin, and 2.2×10^{-16} cm^2 at 20 eV was obtained by Lee and McKoy. These results are considerably larger than both our calculated cross sections and the experimental measurements.

Differential cross sections at selected energies are shown in Fig. 5, along with the experimental measurements of Trajmar at 12.5 and 15 eV [17]. The strong forward scattering seen in this figure is typical of a dipole-allowed transition. The agreement between theory and experiment is fair at 12.5 eV and quite good at 15 eV, especially beyond 30° scattering angle. In the forward direction, however, our results are considerably lower than the experimental measurements, especially at 12.5 eV. This may be partly due to the difference between the theoretical and experimental threshold energies. The threshold energy used here is 1.17 eV higher than the experimental value for this excitation, making the higher partial wave contributions relatively less important and thus leading to less-pronounced forward scattering. This effect is expected to be particularly significant for a dipole-allowed transition. It should be noted that the calculated differential cross section at 15 eV is in better agreement with the measurements at 12.5 eV in the forward direction. On the other hand, if we extrapolate the experimental differential cross sections and integrate over scattering angles, the resulting integral cross sections will be greater than our calculated integral cross sections and thus considerably larger than the experimental measurements of Ajello [8] and of Mumma, Stone, and Zipf [9]. This suggests that either the measured excitation functions are too small or the differential cross sections of Trajmar [17] are too large, especially in the forward direction. Additional comments on the magnitude of the $A\,^1\Pi$ cross sections will be made later.

C. $a'\,^3\Sigma^+$, $e\,^3\Sigma^-$, and $d\,^3\Delta$ states

Our calculated integral cross sections for these three states are shown in Fig. 6. These transitions are dipole forbidden, and the integral cross sections are relatively small. For the $e\,^3\Sigma^-$ and $d\,^3\Delta$ states, the typical character of singlet-to-triplet excitation is seen, i.e., the excitation function rises to a broad maximum and then decreases slowly with increasing electron energy. The maximum is at about 18 eV for each state. For the $a'\,^3\Sigma^+$ state, however, a double-hump structure is seen. The second hump, located at 20 eV, is broad and similar to the maxima for the $e\,^3\Sigma^-$ and $d\,^3\Delta$ states. The origin of the first peak, located at 13.5 eV, is not quite clear. Neither the differential cross section nor the partial wave decomposition shows resonance structure in this energy range. This maximum is probably due to coupling between this state and the $^1\Sigma^+$ state, although further studies will be needed to confirm this.

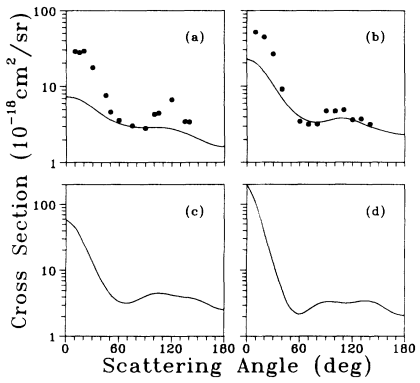

FIG. 5. Same as Fig. 3 but for the $X\,^1\Sigma \rightarrow A\,^1\Pi$ excitation of CO.

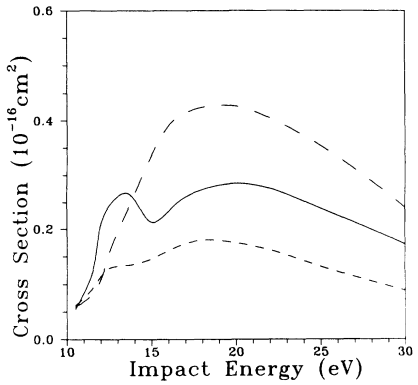

FIG. 6. Integral cross sections for $X\,^1\Sigma \rightarrow a'\,^3\Sigma^+$ (solid line), $e\,^3\Sigma^-$ (short-dashed line), and $d\,^3\Delta$ (long-dashed line) excitations of CO.

The integral cross sections for the $a'\,^3\Sigma^+$ and $d\,^3\Delta$ states have also been calculated by Chung and Lin [18] and by Lee and McKoy [19]. For the $a'\,^3\Sigma^+$ state, a peak value of 1.5×10^{-16} cm^2 at 12 eV was obtained by the former authors, while a peak value of 0.3×10^{-16} cm^2 at 20 eV was obtained by the latter authors. The result of Chung and Lin seems too large, as suggested by Land [2]; the result of Lee and McKoy is in reasonable agreement with ours. For the $d\,^3\Delta$ state, peak values obtained were 0.014×10^{-16} cm^2 at 18 eV by Chung and Lin and 0.032×10^{-16} cm^2 at 20 eV by Lee and McKoy. Both results are considerably smaller than the present values. In these comparisons, we should bear in mind that neither the BOR approximation nor the DW approximation should be reliable at low energy.

To our knowledge, there have been no experimental measurements of the excitation functions for these transitions. However, since carbon monoxide is isoelectronic with N_2 and there are close correspondences between their valence electronic states [40], it may be fruitful to compare the valence electronic excitations of CO to those of N_2. The $a'\,^3\Sigma^+$, $e\,^3\Sigma^-$, and $d\,^3\Delta$ states of CO correlate with the $A\,^3\Sigma_u^+$, $B'\,^3\Sigma_u^-$, and $W^3\Delta_u$ states, respectively, of N_2. The excitation functions for these states of N_2 derived from the measurements of Cartwright *et al.* [41] show maxima around 17 eV impact energy, with maximum values of about 0.21, 0.122, and 0.343×10^{-16} cm^2, respectively. These values are similar to the cross

sections of Fig. 6 for the corresponding states of CO.

We show differential cross sections for these three excitations at selected energies in Figs. 7–9, along with some experimental data of Trajmar [17]. The differential cross sections for the $a'\,^3\Sigma^+$ state show relatively strong scattering in the forward direction at lower energies; with increasing impact energy, scattering in the backward direction becomes more pronounced, as is typical of singlet-to-triplet excitations. A local maximum is seen around 90° scattering angle at all energies, indicating substantial $d\pi$ wave scattering. Indeed, the partial wave composition shows dominant $l=1$ and 2, $m=1$ partial waves in the outgoing channel at all energies considered. The agreement between theory and experiment for this state is quite good, especially at 15 eV. For the $e\,^3\Sigma^-$ state, the differential cross sections are zero at 0° and 180° scattering angles, as expected for $\Sigma^+ \leftrightarrow \Sigma^-$ transitions [42]. For the $d\,^3\Delta$ state, our calculated differential cross sections seem too small and flat.

D. $I\,^1\Sigma^-$ and $D\,^1\Delta$ states

As possible higher-lying metastable states, these two states have been studied in a number of experiments [10–16]. Among the early experiments, the most rigorous was due to Wells, Borst, and Zipf [14]. They located a metastable threshold at 9.5±0.4 eV and determined the state's lifetime to be 97±15 μs. They also gave an excitation function and estimated the peak cross section to be 0.03×10^{-16} cm^2 at 15 eV. The uncertainty of this estimate may be as large as a factor of 3 in magnitude, and the assignment was also uncertain, with possibilities being $I\,^1\Sigma^-$ or $D\,^1\Delta$ or both. Wells, Borst, and Zipf proposed that the assignment could be made clear through further lifetime analyses. A recent experiment of this type was performed by Mason and Newell [16]. In this experiment, similar properties for the metastable state were observed, but it was found that lifetime analysis alone was not enough to make the assignment certain. Through comparisons among experiments and between experimental results and limited theoretical calculations [18,19], Mason and Newell concluded that the $I\,^1\Sigma^-$ state is most likely the metastable state in question.

We have performed calculations for these two transitions and show the integral excitation cross sections in Fig. 10. Since the transitions from the ground state to these two excited states are both dipole forbidden and the excitation energies are relatively high, the cross sections are quite small. For comparison, we include the measured excitation function of Mason and Newell [16] in the same figure. This excitation function is relative, and the maximum was assumed to be 0.03×10^{-16} cm^2 at 16 eV, as estimated by Wells, Borst, and Zipf. The vertical excitation energies in our calculation are 9.7 and 10.14 eV for the $I\,^1\Sigma^-$ and $D\,^1\Delta$ states, respectively; both values are close to the measured threshold for the metastable state. Although the peak cross sections for the $I\,^1\Sigma^-$ and $D\,^1\Delta$ states are, respectively, a factor of 1.9 and a factor of 3.2 larger than that for the measured excitation function (0.03×10^{-16} cm^2), both calculated excitation functions are similar to the measured one in shape. Considering the large uncertainty in the measurement (about a factor of 3 in magnitude as estimated by Wells, Borst, and Zipf), the metastable state seen experimentally can be either $I\,^1\Sigma^-$ or $D\,^1\Delta$ or both states according to our calculation. A similar conclusion was reached by Wells, Borst, and Zipf, as noted above. Further experimental information, such as differential cross sections, is needed to clarify this assignment.

There has been no previous calculation of the cross section for the $X\,^1\Sigma^+ \rightarrow I\,^1\Sigma^-$ transition. Calculations for

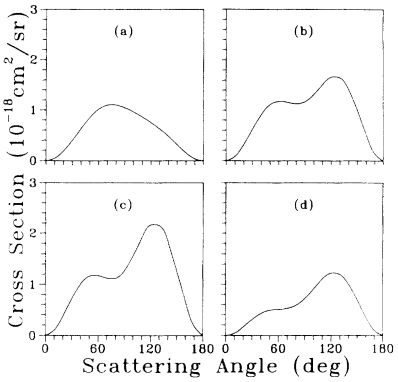

FIG. 8. Differential cross sections for the $X\,^1\Sigma \rightarrow e\,^3\Sigma^-$ excitation of CO at electron-impact energies (a) 12.5 eV; (b) 15 eV; (c) 20 eV; (d) 30 eV.

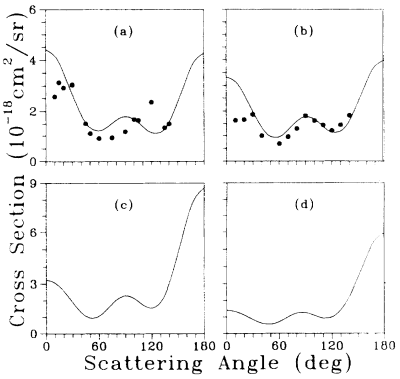

FIG. 7. Same as Fig. 3 but for the $X\,^1\Sigma \rightarrow a'\,^3\Sigma^+$ excitation of CO.

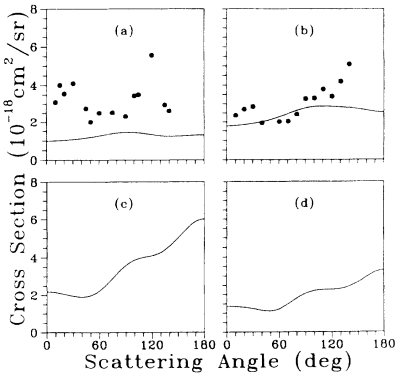

FIG. 9. Same as Fig. 3 but for the $X\,^1\Sigma \rightarrow d\,^3\Delta$ excitation of CO.

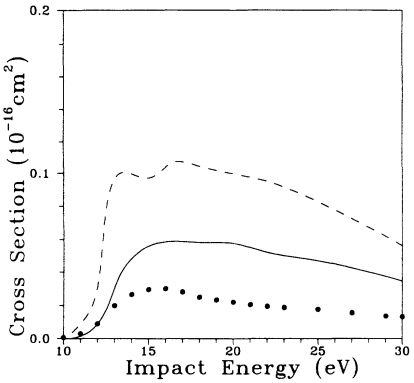

FIG. 10. Integral cross sections or $X\,^1\Sigma \rightarrow I\,^1\Sigma^-$ (solid line) and $D\,^1\Delta$ (dashed line) excitations of CO. The dots are the experimental measurements of Mason and Newell, Ref. [16], for an unassigned higher-lying metastable state of CO.

the $X\,^1\Sigma^+ \rightarrow D\,^1\Delta$ transition were done by Chung and Lin [18] and by Lee and McKoy [19]. The integral cross sections of both calculations are about a factor of 5 larger than ours and thus are much larger than the observed metastable excitation function.

The differential cross sections are very distinct for these two states, as seen in Figs. 11 and 12. The differential cross sections for the $D\,^1\Delta$ state are fairly flat and unstructured at lower energies but show some backward scattering and structures at higher energies. The differential cross sections for the $I\,^1\Sigma^-$ state are zero at 0° and 180° scattering angles, reflecting the $\Sigma^+ \leftrightarrow \Sigma^-$ selection rule [42]. Such differential cross sections, if measured, can aid in identifying the metastable state in question. It is also interesting to note that the ratio of the triplet to the singlet cross sections is about 3 for both Σ^- and Δ states. The same ratio was observed for the forbidden transitions from the ground state to the $a\,^3A_2$ and $A\,^1A_2$ states of formaldehyde [25].

E. Total electronic excitation cross section

The sum of the integral excitation cross sections for all the valence states studied here is plotted in Fig. 13. For comparison, the recommended total electronic excitation cross section of Kanik, Trajmar, and Nickel [43] is plotted in the same figure. The latter is obtained by subtracting measured elastic, vibrationally inelastic, and ionization cross sections from the measured total cross section and by empirical estimates. Several points may be made about this comparison. First, good agreement between the present and the estimated total excitation cross section is seen below 12 eV. Since the excitation to the $a\,^3\Pi$ state dominates below 10 eV, this good agreement may suggest that both the magnitude and the shape of the calculated excitation function for this state are reasonable at these energies. Second, our calculated total excitation function is almost always below the estimated one (except for one point at 10.5 eV). Finally, the calculated total excitation function is considerably smaller than the estimated one above 15 eV. This is certainly due in part to the neglect of excitations to the Rydberg states.

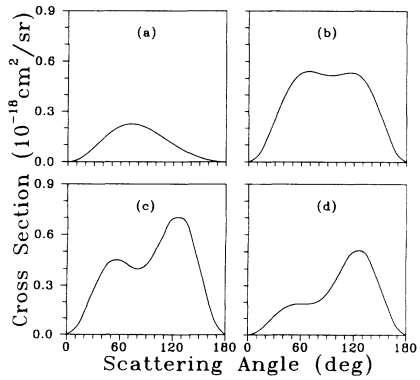

FIG. 11. Same as Fig. 8 but for the $X\,^1\Sigma \rightarrow I\,^1\Sigma^-$ excitation of CO.

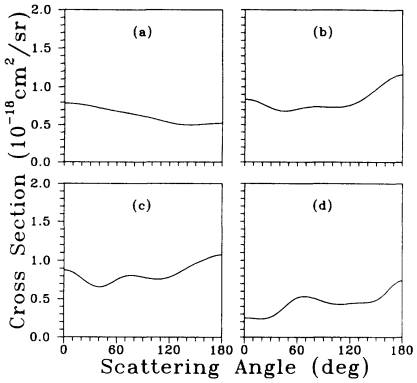

FIG. 12. Same as Fig. 8 but for the $X\,^1\Sigma \rightarrow D\,^1\Delta$ excitation of CO.

V. SUMMARY AND CONCLUSIONS

We have carried out *ab initio* calculations of the cross sections for electron-impact excitation of the valence states of carbon monoxide using the SMC method. Both differential and integral cross sections were obtained. The integral cross sections were compared to various ex-

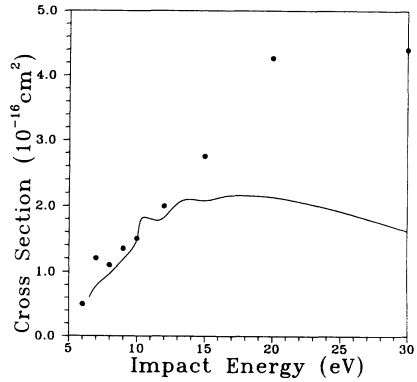

FIG. 13. Total electronic excitation cross section of CO. The solid line is the present result including all valence excitations; the dashed line is the result recommended by Kanik, Trajmar, and Nickel (Ref. [43]).

perimental excitation functions, and reasonable agreement was found. The differential cross sections were compared to the absolute measurements of Trajmar at 12.5 and 15 eV, and fairly good agreement was found for the $a\ ^3\Pi$, $A\ ^1\Pi$, and $a'\ ^3\Sigma^+$ states, although the agreement for the $D\ ^3\Delta$ was poor. While there have not yet been any measurements of the differential cross sections for the $e\ ^3\Sigma^-$, $I\ ^1\Sigma^-$, and $D\ ^1\Delta$ states, the Σ^- differential cross sections were found to be zero at 0° and 180°, correctly reflecting the $\Sigma^+ \leftrightarrow \Sigma^-$ selection rule. In addition, the total electronic excitation cross section in the low-energy range was estimated. The present calculation illustrates that such quantities can be obtained fairly easily in the low-energy range using *ab initio* methods.

ACKNOWLEDGMENTS

This work was done on the Intel Touchstone Delta system operated by the Concurrent Supercomputing Consortium (CSCC) and on the CRAY Y-MP2E/116 of the Jet Propulsion Laboratory (JPL)/California Institute of Technology Supercomputing Project. We thank Dr. Heidi Lorenz-Wirzba of the CSCC and Dr. Edith Huang of JPL for technical assistance and Dr. S. Trajmar of JPL for providing the unpublished results of Refs. [17] and [43]. Financial support from the National Science Foundation under Grant No. PHY-9021933, and from the Innovative Science and Technology Program of the Strategic Defense Initiative Organization through the Army Research Office, is gratefully acknowledged.

*Present address: Biosym Technologies, 9685 Scranton Road, San Diego, CA 92121.

[1] E. W. McDaniel and W. L. Nigham, Appl. At. Collision Phys. **3**, 294 (1982).
[2] J. E. Land, J. Appl. Phys. **49**, 5716 (1978).
[3] S. Saha, S. Ray, B. Bhattacharyya, and A. K. Barua, Phys. Rev. A **23**, 2926 (1981); G. P. Menees, J. Spacecraft Rockets **22**, 37 (1985); D. M. Cooper, R. L. Jaffe, and J. O. Arnold, *ibid.* **22**, 60 (1985).
[4] M. Allan, J. Electron Spectrosc. Relat. Phenom. **48**, 219 (1989), and references cited therein.
[5] S. Trajmar, D. F. Register, and A. Chutjian, Phys. Rep. **97**, 219 (1983), and references cited therein.
[6] H. H. Brongersma, A. J. H. Boerboom, and J. Kistemaker, Physica **44**, 419 (1969).
[7] D. S. Newman, M. Zubek, and G. C. King, J. Phys. B **16**, 2247 (1983).
[8] J. Ajello, J. Chem. Phys. **55**, 3158 (1971).
[9] M. J. Mumma, E. J. Stone, and E. C. Zipf, J. Chem. Phys. **54**, 2627 (1971).
[10] J. Olmsted, A. S. Newton, and K. Street, J. Chem. Phys. **42**, 2321 (1965).
[11] V. Cermak, J. Chem. Phys. **44**, 1318 (1966).
[12] W. L. Borst and E. C. Zipf, Phys. Rev. A **3**, 979 (1971).
[13] W. L. Borst, Phys. Rev. A **5**, 648 (1972).
[14] W. C. Wells, W. L. Borst, and E. C. Zipf, Phys. Rev. A **8**, 2463 (1973).
[15] J. N. H. Brunt, G. C. King, and F. H. Read, J. Phys. B **11**, 173 (1978).
[16] N. J. Mason and W. R. Newell, J. Phys. B **21**, 1293 (1988).
[17] S. Trajmar (unpublished).
[18] S. Chung and C. C. Lin, Phys. Rev. A **9**, 1954 (1974).
[19] M. Lee and V. McKoy, J. Phys. B **15**, 3971 (1982).
[20] K. Takatsuka and V. McKoy, Phys. Rev. A **24**, 2473 (1981); **30**, 1734 (1984).
[21] W. M. Huo, T. L. Gibson, M. A. P. Lima, and V. McKoy, Phys. Rev. A **36**, 1632; **36**, 1642 (1987).
[22] M. A. P. Lima, L. M. Brescansin, A. J. R. da Silva, C. Winstead, and V. McKoy, Phys. Rev. A **41**, 327 (1990), and references cited therein.
[23] P. G. Hipes, C. Winstead, M. A. P. Lima, and V. McKoy, in *Proceedings of the Fifth Distributed Memory Computing Conference, Vol. I: Applications,* edited by D. W. Walker and Q. F. Stout (IEEE Computer Society, Los Alamitos, CA, 1990), p. 498; C. Winstead, Q. Sun, P. G. Hipes, M. A. P. Lima, and V. McKoy, Aust. J. Phys. **45**, 325 (1992).
[24] Q. Sun, C. Winstead, V. McKoy, and M. A. P. Lima, J. Chem. Phys. **96**, 3531 (1992).
[25] Q. Sun, C. Winstead, V. McKoy, J. S. E. Germano, and M. A. P. Lima, Phys. Rev. A **46**, 2462 (1992).
[26] C. Winstead, P. G. Hipes, M. A. P. Lima, and V. McKoy, J. Chem. Phys. **94**, 5455 (1991); C. Winstead, Q. Sun, and V. McKoy, *ibid.* **96**, 4246 (1992); C. Winstead, Q. Sun, V. McKoy, J. S. E. Germano, and M. A. P. Lima, Z. Phys. D (to be published).
[27] A. W. Fliflet and V. McKoy, Phys. Rev. A **21**, 697 (1980).
[28] O. H. Crawford, A. Dalgarno, and P. B. Hays, Mol. Phys. **13**, 181 (1971).
[29] T. N. Rescigno and B. I. Schneider, Phys. Rev. A **45**, 2894 (1992).
[30] T. H. Dunning, J. Chem. Phys. **53**, 2823 (1970).
[31] W. M. Huo, J. Chem. Phys. **43**, 624 (1965).
[32] *CRC Handbook of Chemistry and Physics,* 58th ed., edited by R. C. Weast (CRC, Cleveland, 1978), p. E-63.
[33] W. A. Goddard and W. J. Hunt, Chem. Phys. Lett **24**, 464 (1974).
[34] V. D. Meyer, A. Skerbele, and E. N. Lassettre, J. Chem. Phys. **43**, 805 (1965).
[35] G. Herzberg, T. Hugo, S. Tilford, and J. Simmons, Can. J. Phys. **48**, 3004 (1970).
[36] P. H. Krupenie, *The Band Spectrum of Carbon Monoxide,* Natl. Std. Ref. Data Ser., Natl. Bur. Std. No. 5 (U.S. GPO, Washington, DC, 1966), p. 1.
[37] L. Chantranupong, K. Bhanuprakash, M. Honigmann, G. Hirsch, and R. T. Buenker, Chem. Phys. **161**, 351 (1992).
[38] M. Eidelsberg, F. Rostas, J. Breton, and B. Thieblemont, J. Chem. Phys. **96**, 5585 (1992).
[39] C. Winstead and V. McKoy, Phys. Rev. A **41**, 49 (1990).
[40] J. B. Rose and V. McKoy, J. Chem. Phys. **55**, 5435 (1971).
[41] D. C. Cartwright, A. Chutjian, S. Trajmar, and W. Williams, Phys. Rev. A **16**, 1013 (1977); **16**, 1041 (1977).
[42] D. C. Cartwright, S. Trajmar, W. Williams, and D. L. Huestis, Phys. Rev. Lett. **27**, 704 (1971).
[43] I. Kanik, S. Trajmar, and J. C. Nickel, J. Geophys. Res. (to be published).